# Controllable Synthesis of Monodisperse $CaF_2$ microsphere and the Investigation on luminous performance of $CaF_2$:$Ce^{3+}$/$Tb^{3+}$

X. Sun[*], X. Hu[*,**], J. Fan[***], S. Zhan[*], Y. Wang[*], Z. Wang[*], Q. Sun[*], Y. Hao[*]

[*]School of Physics, Northwest University, 710069, P. R. China.
[**]State Key Laboratory of Transient Optics and Technology, Xi'an Institute of Optics & Precision Materials, Chinese Academy of Science, Xi'an 710068, China.
[***]School of Chemical Engineering, Xi'an, 710069, P. R. China.
Corresponding author Email: hxy3275@nwu.edu.cn

## ABSTRACT

In this paper, highly uniform and well-dispersed $CaF_2$ microsphere with tunable particles size have been successfully synthesized by a facile hydrothermal process using ethylenediaminetetraacetic acid disodium as a complexing reagent. The XRD results indicated that the as-prepared microspheres were of cubic phases and had good crystallinity and purity. The TEM and SEM results reveal that monodisperse and uniform hollow sphere with rough surfaces can be prepared by this approach. In addition, $Ce^{3+}$/$Tb^{3+}$-codoped $CaF_2$ sphere can be prepared similarly. Excitation and emission spectra are shown that the samples can absorb ultraviolet light and emit light at 335 nm. In the emission spectrum, it is clear that emission intensity of $Ce^{3+}$ decreases with increasing $Tb^{3+}$, it shows that efficient energy transfer from $Ce^{3+}$ to $Tb^{3+}$ may occur. It significantly improves the absorption range and intensity of the samples. That is extremely useful and has potential application value in display, light, laser, optical information transfer, scintillator and optoelectronic devices.

***Keywords***: $CaF_2$, hollow microsphere, energy transfer, rare earth ions doping, luminescence

## 1 INTRODUCTION

Physical and chemical properties of luminescence materials vary drastically with the sizes and shapes. Nanomaterials with controllable sizes and shapes have attracted great interest because of their unique properties and potential applications. The fluoride nanomaterials have a variety of shapes and can obtained different sizes of particles. What's more, the fluoride nanomaterials have a wide range of potential applications due to their high transparency arising from low energy phonons and high iconicity, which leads to less fundamental adsorption than other oxide or sulphide materials. Among the various fluorides, calcium fluoride ($CaF_2$) nanomaterials with various morphologies have been successfully fabricated by changing the conditions, such as nanoparticles, nanocubes, thin films[2]. $CaF_2$ nanomaterial has a low refractive index and is optically transparent over a wide wavelength range from mid-infrared to vacuum ultraviolet. So it has been used in UV-transparent optical lenses, biocompatible luminescent markers and so on. $CaF_2$ is also a well-known host for luminescent ions due to its high transparency in a broad wavelength range, low phonon energy and a wide band gap ($E_g$=12.1eV)[1]. Which display unique down-conversion luminescence properties arising from their 4f electron configuration. However, the studies on the lanthanide (III)-doped $CaF_2$ nanomaterials is scare, especially with controllable morphologies in a mild reaction conditions.

## 2 EXPERIMENTAL

### 2.1 Hydrothermal synthesis of $CaF_2$ and $CaF_2$:$Ce^{3+}$/$Tb^{3+}$ nanomaterials

In this work, $CaF_2$ nanoparticles were prepared hydro-thermally. All the chemical reagents used were analytical grade. Including calcium nitrate ($Ca(NO_3)_3$ $4H_2O$), ethylenediaminetetraacetic acid disodium (EDTA-2Na), sodium fluoborate（$NaBF_4$）, ammonia water($NH_3$ $nH_2O$), deionized water and ethanol. Calcium nitrate was dissolved in 30ml deionized water to form a solution. Then ethylenediaminetetraacetic acid disodium was added to the above solution under vigorous stirring until clear to form solution I. $NaBF_4$ solution was then prepared by dissolving $NaBF_4$ in deionized water in a beaker to form solution II. It was gradually added solution II into solution I while being stirred at room temperature. The pH value of the final solution was adjusting to 6.0 with ammonia water. The final mixture was kept in an autoclave at 160℃ for 5h. The resulting product was collected by centrifuge at 8000rpm, for 10min, and washed several times in a thorough manner using deionized water and ethanol. At last dry them in vacuum at 60℃ for 24h.

Rare-earth ions such as $Ce^{3+}$ or $Tb^{3+}$ doped $CaF_2$ samples were prepared by the same procedure, except that an additional cerous nitrate ($Ce(NO_3)_3$) and terbium nitrate ($Tb(NO_3)_3$) added into solution I first.

## 2.2 Characterization of $CaF_2$ samples

Phase identification was performed via powder X-ray diffraction ( XRD ) ( Rigaku D/MAX-2400 ) with CuKα radiation (λ = 0.154178 nm). The morphology and elementary composition were characterized by the Quamta400 FEG thermal environment scanning electron microscope (SEM). TEM images were taken with a transmission electron microscopy (TEM). Samples for TEM were obtained by dispelsing the products in ethanol with 15 min ultrasounding, and then dropping a few drops of the resulted suspension onto a copper grid precoated with amorphous carbon and allowing them to dry naturally. Excitation and emission spectra were examined with a Hitachi F-7000 fluorescence spectrometer equipped with a continuous 150-W Xenon lamp as the excitation source at room-temperature. To compare the intensity of different specimens, the emission spectra were measured with the same instrument parameters (2.5 nm for excitation slit, 2.5 nm for emission slit, and 350-V for PMT voltage).

# 3 RESULTS AND DISCUSSION

## 3.1 The XRD characterization of $CaF_2$ and $CaF_2:Ce^{3+}/Tb^{3+}$ samples

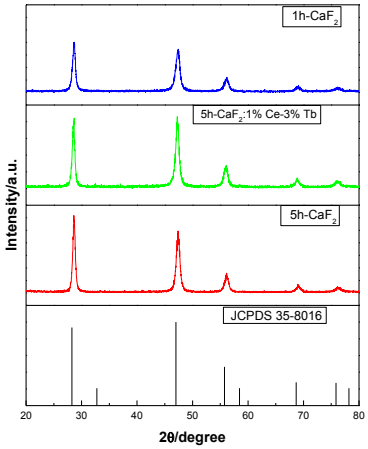


**Fig.1.** XRD pattern of the as-prepared samples

The crystal structure and the phase purity of the product were determined by X-ray diffraction (XRD). A typical XRD pattern of the as-prepared sample is presented in Fig.1. All of the diffraction peaks of the XRD pattern can be indexed as pure cubic phase, and coincide well with the standard data of $CaF_2$ (JCPDS 35-0816). When the reaction time extends to 1 h or longer, all diffraction peaks of the as-obtained samples can be indexed to the cubic phase of $CaF_2$. That means pure $CaF_2$ is formed. The diffraction peaks of the $CaF_2$ samples become sharper and stronger with increasing reaction time. That means the nanoparticles grow gradually, and the crystallinity increases with increasing reaction time. To compare with the XRD of $CaF_2:Ce^{3+}/Tb^{3+}$ samples, there is no diffraction peaks from $CeF_3$ or $TbF_3$ which may exist as impurities. Suggesting that $Ce^{3+}/Tb^{3+}$ were successfully doped into $CaF_2$ matrix in this route. The high and sharp peaks indicate that the samples were well crystallized and purity.

## 3.2 SEM and TEM characterization of $CaF_2$ samples

The SEM image of the as-prepared $CaF_2$ sample (Figure.2.a) shows that monodisperse and uniform spheres can be prepared by this approach. The diameters of the spheres are about 350 nm. The yield of the spheres is closed to 100%. The TEM image (Figure.2.b) provides detailed structural information of the spheres. It shows that the $CaF_2$ spheres are hollow structure with rough surfaces which contains of numerous interlaced nanosheets. Figure.2.c shows a typical TEM image of the $CaF_2$ hollow spheres, which further confirms the uniform size and hollow structure of the $CaF_2$ spheres. The high-magnification TEM image in Figure.2.d shows the edge structure clearly of the hollow sphere. It shows the stacking of the building blocks and the interior cavity of the sphere, since the contrast at the center is much lower than that of a solid particle. We further confirm that the $CaF_2$ nanomaterials were hollow structure.

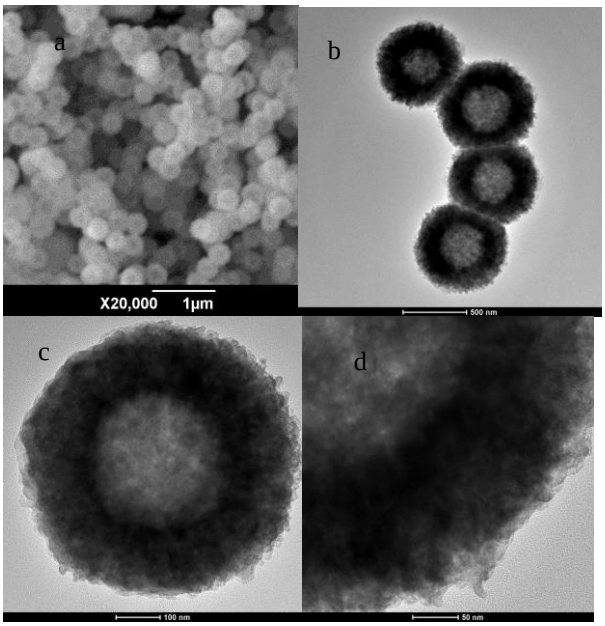


**Fig.2.** SEM and TEM images of the $CaF_2$ sample

Figure 3 shows the SEM image of the $CaF_2$ sample prepared without EDTA as the complexing agent. It can be seen that there is no obvious consistent with the above samples in figure.2. The as-synthesized $CaF_2$ sample was composed of irregular particles on a large scale. During the process, EDTA plays a critical role in controlling the morphology of the final $CaF_2$ products.

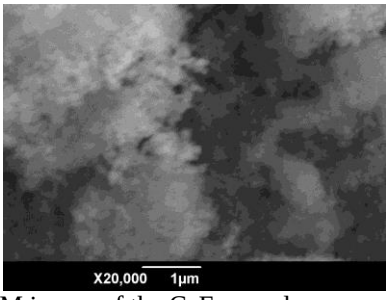


**Fig.3.** SEM image of the $CaF_2$ sample prepared without EDTA

The detailed formation process of the $CaF_2$ hollow spheres can be summarized as follows.

$Ca^{2+}$+Edta→$Ca^{2+}$-Edta(complex sphere)
$BF_4^-$+3$H_2O$→3H F +$F^-$+$H_3BO_3$
$Ca^{2+}$-Edta+2$F^-$→$CaF_2$+ Edta

As an efficient chelator for $Ca^{2+}$, Edta could react with $Ca^{2+}$ to form stable $Ca^{2+}$-Edta complex sphere. The as-obtained intermediate was employed as both physical and chemical template, which not only cast the morphology of the product but also afforded a reactant source for an interfacial reaction. The hydrolysis of $NaBF_4$ was a slow process. $F^-$ ions were slowly produced by hydrolysis of $NaBF_4$. Then $F^-$ reacted with $Ca^{2+}$ to form $CaF_2$ nanoparticles. The $CaF_2$ nanoparticles further agregate to form $CaF_2$ shells. The $CaF_2$ nuclei were formed by surface deposition and a subsequent crystal growth process, during which $F^-$ deposited onto the surface of the intermediate solid spheres and reacted with the inner core to generate $CaF_2$ nuclei. With further reaction, $CaF_2$ hollow spheres are obtained by evacuation of the intermediate solid spheres, which is believed to be the result of the Ostwald ripening mechanism[3] induced by a chemical transformation. Once the cores in the center of the microspheres are consumed completely, hollow spheres are formed.

Figures.4. shows SEM images of the $CaF_2$ samples at different pH values. The size of the hollow $CaF_2$ spheres is critically dependent on the pH value during the hydrothermal process. When the pH value of the initial solution is adjusted to 3.0, the size of the hollow spheres decreases to about 100 nm. When the pH value is 6.0, the size of the hollow spheres is about 300 nm. When the pH value of the initial solution is adjusted to 8.0, the size of the hollow spheres increases to about 900 nm and the hollow structure become solid spheres. The size of the $CaF_2$ can be controlled from 100nm to 900nm by adjusting the pH value.

## 3.3 Photoluminescence properties of $CaF_2$:$Ce^{3+}$/$Tb^{3+}$ hollow spheres

All of the $CaF_2$:$Ce^{3+}$-$Tb^{3+}$ samples exhibit a strong green emission under UV excitation. The $CaF_2$:$Ce^{3+}$ sample shows UV emission centered at 335 nm on UV excitation (306 nm). The excitation and emission spectra of $CaF_2$:$Ce^{3+}$ are shown in Figure.5 (a, b). The excitation spectrum (Figure.5.a) consists of abroad and strong band with a maximum at 300 nm and a weaker band at 250 nm, which corresponds to the transitions from the $^2F_{5/2}$ ground state of $Ce^{3+}$ to the different components of the excited $Ce^{3+}$ 5d states split by the crystal field.

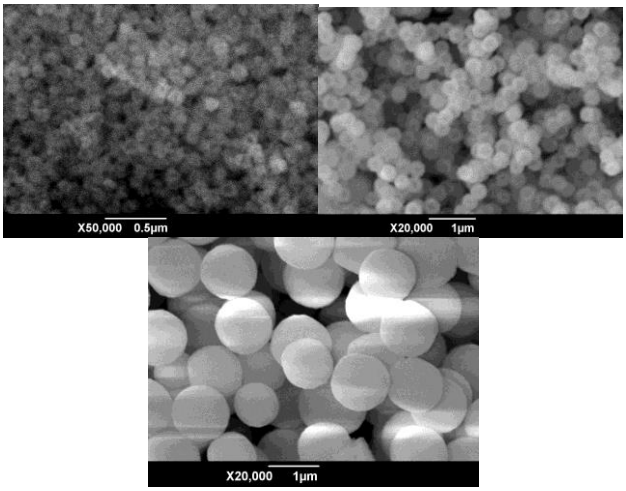


**Fig.4.** SEM image of the $CaF_2$ samples at different pH values.pH=3，6，8

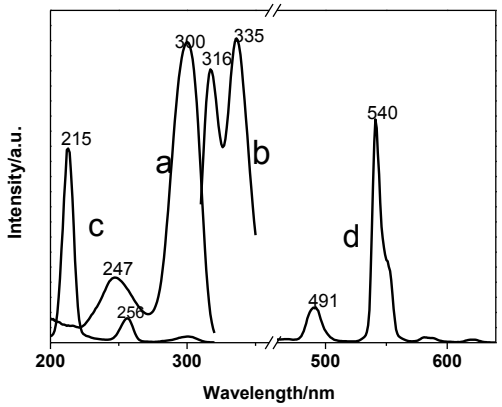


Fig.5. Excitation and emission spectra for $CaF_2$:$Ce^{3+}$(a, $\lambda_{em}$=335nm;b, $\lambda_{ex}$ =300nm) and $CaF_2$:$Tb^{3+}$ (c, $\lambda_{em}$ =540nm;d, $\lambda_{ex}$ =215nm)

The emission spectrum of $Ce^{3+}$ (Figure.5.b) consists of two peaks at 316 and 335 nm respectively, which corresponds to the transitions from the lowest excited 5d state to the 4f ground state, and the doublet is a result of the ground-state splitting, that is, the $^2F_{5/2}$ and $^2F_{7/2}$ levels of $Ce^{3+}$. This splitting, which is calculated to be about 1700 /cm, approaches the theoretical value of 2000 /cm. The excitation spectrum of $CaF_2$:$Tb^{3+}$ (Figure.5.c) consists of a strong band at 215 nm and a weak band at 256 nm, which respectively correspond to the components of the $4f^8$–$4f^7$5d transition. The emission spectrum of $Tb^{3+}$ (Fig.5.d) exhibits four peaks centered at 491, 540, 580, 621 nm[5],

respectively, originating from transitions from the $^5D_4$ excited state to the $^7F_J$ (J=6, 5, 4,3) ground states of $Tb^{3+}$, among which the $^5D_4$-$^7F_4$ transition at 540 nm is the most prominent.

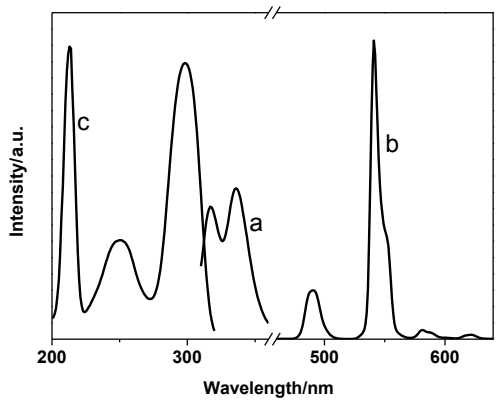


**Fig.6.** Excitation and emission for $CaF_2$:$Ce^{3+}$-$Tb^{3+}$(a, b, $\lambda_{ex}$ =300 nm; c, $\lambda_{em}$ =540 nm;)

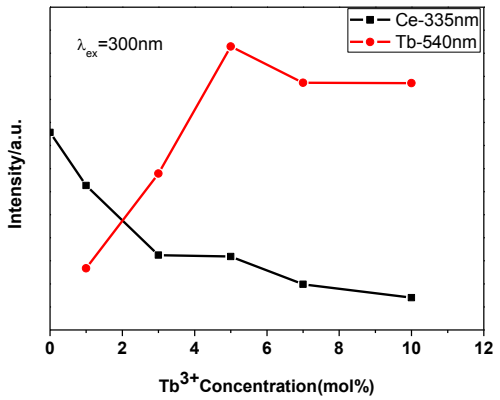


**Fig.7.** The intensities of $Ce^{3+}$ 300 nm and $Tb^{3+}$ 542 nm emissions as a function of $Tb^{3+}$ concentration in $CaF_2$:$Ce^{3+}$-$Tb^{3+}$samples

Figure.6. a, b, c show the excitation and emission spectra of the $Ce^{3+}$/$Tb^{3+}$-codoped $CaF_2$ sample. The excitation spectrum (Figure.6.c) monitored at the 541 nm contains a strong band at 215 nm, a weak band at 256 nm, and a strong broad band with a maximum at 300 nm. In comparison with the excitation spectra of $CaF_2$:$Ce^{3+}$ and $CaF_2$ $Tb^{3+}$ samples in figure.5. , we can draw a conclusion that the excitation band at 300 nm is corresponding to 5d - 4f transition of $Ce^{3+}$ ions. It indicates that energy transfer occurs from $Ce^{3+}$ to $Tb^{3+}$ in $CaF_2$:$Ce^{3+}$-$Tb^{3+}$. In the emission spectra, it is clear that emission intensity of $Ce^{3+}$ decreases while the intensity of $Tb^{3+}$ increases with increasing $Tb^{3+}$ (Fig.7.), this can also improve that energy transfer from $Ce^{3+}$ to $Tb^{3+}$ may occur. And the maximum sensitivity is obtained at about 5mol% of $Tb^{3+}$ concentration.

## 4 CONCLUSIONS

In this work, nanoparticles of $CaF_2$ and $Ce^{3+}$/$Tb^{3+}$-codoped $CaF_2$ hollow spheres were synthesized by a simple synthetic method. The TEM and SEM characterization showed that the obtained hollow spheres were highly uniform and well-dispersed which is suitable for use as drug carrier. For $Ce^{3+}$/$Tb^{3+}$-codoped $CaF_2$ samples, a strong green emission at about 541 nm can be observed under UV excitation. And it is clear that energy transfer occurs from $Ce^{3+}$ to $Tb^{3+}$ in $CaF_2$:$Ce^{3+}$-$Tb^{3+}$. The as-obtained mono-disperse $CaF_2$:$Ce^{3+}$-$Tb^{3+}$ hollow spheres can thus be used to encapsulate chemicals and release them. These materials may find potential applications in the fields of luminescence, drug delivery, and disease therapy, based on their well-dispersed and uniform luminescent and mesoporous properties.

## ACKNOWLEDGEMENTS

This work has been supported by the National Natural Science Foundation of China (Grant No. 51372201, 21176199), the Research Fund for the Doctoral Program of Higher Education (Grant No. 20136101110009)， the Research Foundation for the Industrialization Cultivation Item of Shaanxi Province Educational Department (Grant No.2011JG05，12JK0977).

## REFERENCES

[1] M. Zahedifar, E. Sadeghi, M.R. Mozdianfard, "Synthesis, characteristics and thermolumin-escent dosimetry features of γ-irradiated Ce doped $CaF_2$ nanophosphor, " Applied Radiation and Isotopes, 78, 125–131, 2013.

[2] Lin Ma, Lin-Lin Yang, Yong-Gang Wang, Xiao-Ping Zhou, "Microwave-assisted preparation of nearly monodisperse flower-like $CaF_2$ microspheres, " Ceramics International,39, 5973–5977,2013.

[3] K.Chen, S.H.Sun, "Recent advances in syntheses and therapeutic applications of multifunctional porous hollow nanoparticles," Nano Today, 5,183-196, 2012.

[4] A. Bensalaha, M.Mortiera, G.Patriarcheb, P.Gredinc, D.Vivien, "Synthesis and optical characterizations of un-doped and rare-earth-doped $CaF_2$ nanoparticles, " Journal of Solid State Chemistry, 179, 2636–2644, 2006.

[5] Limei Song, Lei Xue, "Efficient fluorescence of dissolved $CaF_2$:$Tb^{3+}$and $CaF_2$:$Ce^{3+}$, $Tb^{3+}$ nano-particles through surface coating sensitization, " Applied Surface Science, 258,, 3497–3501, 2012.

[6] Xiaoying Yang, Bo Huang, Xinlin Yang, "Synthesis of pH-sensitive hollow polymer microspheres and their application as drug carriers, " Polymer, 50, 3556–3563, 2009.